China Ocean Eng., Vol. 30, No. 5, pp.718 – 732

DOI 10.1007/s13344-016-0046-2, ISSN 0890-5487

Development of A Depth-Integrated Longshore Current Model with Unstructured Grids

CHEN Chao (陈 超) and ZHANG Qing-he (张庆河)[1]

State Key Laboratory of Hydraulic Engineering Simulation and Safety, *Tianjin University*, *Tianjin 300072*, *China*

(Received 18 July 2014; received revised form 8 May 2015; accepted 20 June 2015)

ABSTRACT

A depth-integrated model for simulating wave-induced longshore current was developed with unstructured grids. Effects of surface roller and horizontal mixing under combined waves and currents were incorporated in the numerical model. Recommended values of model coefficients were also proposed based on sensitivity analysis. Field observations and three series of laboratory measurements including two cases conducted on the plane beach and one implemented on the ideal inlet were employed to examine the predictive capability of this model. For the field case and laboratory cases conducted on the plane beach, numerical results were compared favorably with the measured data. For the case with an ideal inlet, simulated circulation pattern is supposed to be reasonable although some deviations between numerical results and measured data still can be detected.

Key words: *longshore current*; *numerical model*; *unstructured grids*; *surface roller*; *horizontal mixing*

1. Introduction

Wave-induced longshore current is usually the major driving force for sediment transport and morphology change on sandy coasts, especially on condition that the long-term shoreline evolution is focused. For estimating shoreline evolution at the time scale of years or decades, a great many numerical models have been developed based on total longshore sediment transport across the surf zone (e.g. Dabees and Kamphuis, 1998; Murray and Aston, 2004; Artagan, 2006). However, most of these studies applied the one-line model assuming that longshore sediment transport rate is uniform across the surf zone and the beach profile parallels itself during shoreline erosion or accumulation. From an accurate simulation point of view, it is supposed to be preferable to include cross-shore distribution of longshore sediment transport in shoreline evolution models. It is evident that the distributed pattern of longshore sediment transport depends significantly on the cross-shore profile of longshore currents in the surf zone. Hence, a numerical model of wave-induced longshore currents should be developed as a prerequisite for evaluating the distributed longshore sediment transport rate.

In the past few years, both depth-integrated (Sun *et al*., 2002; Cui *et al*., 2008; Nam *et al*., 2009; Baykal *et al*., 2014) and three-dimensional numerical models (Ding *et al*., 2006; Treffers, 2008; Zheng and Tang, 2009; Zheng *et al*., 2012) for investigating wave-induced currents have been developed. Obviously, high accuracy and vertical structure of longshore currents could be obtained from three-

1 Corresponding author. E-mail: coastlab@163.com

dimensional models. Besides, physical processes are much clearer in fully three-dimensional simulation compared with depth-integrated models. However, in long-term simulation of longshore sediment transport and shoreline evolution involving longshore currents, three-dimensional models are actually time-consuming and impractical. Therefore, it motivates us to develop a depth-integrated numerical model of wave-induced longshore currents. Results of this work will be applied to investigate distributed longshore sediment transport and long-term shoreline evolution in the future.

Basically, most of depth-integrated models of longshore currents were developed based on the concept of radiation stress proposed by Longuet-Higgins and Stewart (1962). Longuet-Higgins (1970) reported that both the bottom friction and the horizontal mixing were essential in evaluating longshore currents, which was also accepted and validated by many researchers. After that, Smith *et al*. (1993) and Kuriyama and Ozaki (1993) found that the peak value of longshore current velocity was always shoreward of the bar crest in the field which could not be predicted by traditional models. Following the concept of surface roller reported by Svendsen (1984a), Reniers and Battjes (1997), Goda (2006) and Zheng and Tang (2009) presented that significant shoreward shift of the peak value of longshore velocity could be obtained by incorporating effects of surface roller in their models. Additionally, Zhang *et al*. (2009) incorporate effects of surface roller in the prediction of undertow. More recently, Zheng *et al*. (2014) have demonstrated the importance of surface roller in modeling undertow and investigated the effects of roller slope systematically. Therefore, it is believed that effects of surface roller are essential in simulating wave-induced currents.

In most of the depth-integrated models, the method of evaluating horizontal mixing terms and roller effects are different. Even though the same formula is employed, the value of the empirical coefficient involved is still equivocal. Expressions of the horizontal mixing term and the surface roller are needed to be further investigated. Moreover, most existing models of longshore currents are based on structured grids with very few exceptions such as that presented by Cui *et al*. (2011) with curvilinear meshes and Zhang *et al*. (2012) with quadtree grids. Coastlines and topography in the surf zone are usually irregular and complex in practice. Employing unstructured-grids would be a flexible way to describe the complex topography especially when engineering structures such as breakwaters and jetties are included in the simulated area.

The major objectives of the present study are to develop a depth-integrated, unstructured-grid model of wave-induced longshore current including effects of surface roller and horizontal eddy viscosity and to examine the performance of this model with fixed model coefficients. Field observations, laboratory measurements conducted on a plane beach and the physical model implemented on an ideal inlet with jetties were employed to examine the predictive capability of this model.

This paper is organized as follows. In the second section, governing equations and expressions for the radiation stress, effects of the surface roller, horizontal mixing terms and the bottom shear stress are described. In the third section, the kinetic energy of the surface roller and empirical coefficients in calculating wave-induced horizontal mixing are studied through sensitivity tests. The model is verified by laboratory observations and field data in the fourth part. Finally, some conclusions are presented.

2. Numerical Model

2.1 Governing Equations

In the present study, the depth-integrated model of longshore current is developed based on the unstructured-grid, finite-volume coastal ocean model FVCOM (Chen *et al*., 2003), in which the continuity equation and momentum equations are described as follows:

$$\frac{\partial \eta}{\partial t}+\frac{\partial (hu)}{\partial x}+\frac{\partial (hv)}{\partial y}=0\,; \tag{1a}$$

$$\frac{\partial (hu)}{\partial t}+\frac{\partial (hu^2)}{\partial x}+\frac{\partial (huv)}{\partial y}+gh\frac{\partial \eta}{\partial x}=-\frac{1}{\rho}\left(\frac{\partial S_{xx}}{\partial x}+\frac{\partial S_{xy}}{\partial y}\right)-\frac{1}{\rho}\left(\frac{\partial R_{xx}}{\partial x}+\frac{\partial R_{xy}}{\partial y}\right)$$
$$-\frac{1}{\rho}\tau_{bx}+h\frac{\partial}{\partial x}\left(2\nu_{cw}\frac{\partial u}{\partial x}\right)+h\frac{\partial}{\partial y}\left[\nu_{cw}\left(\frac{\partial u}{\partial y}+\frac{\partial v}{\partial x}\right)\right]; \tag{1b}$$

$$\frac{\partial (hv)}{\partial t}+\frac{\partial (huv)}{\partial x}+\frac{\partial (hv^2)}{\partial y}+gh\frac{\partial \eta}{\partial y}=-\frac{1}{\rho}\left(\frac{\partial S_{yx}}{\partial x}+\frac{\partial S_{yy}}{\partial y}\right)-\frac{1}{\rho}\left(\frac{\partial R_{yx}}{\partial x}+\frac{\partial R_{yy}}{\partial y}\right)$$
$$-\frac{1}{\rho}\tau_{by}+h\frac{\partial}{\partial x}\left[\nu_{cw}\left(\frac{\partial v}{\partial x}+\frac{\partial u}{\partial y}\right)\right]+h\frac{\partial}{\partial y}\left(2\nu_{cw}\frac{\partial v}{\partial y}\right), \tag{1c}$$

where, η means the water level; u and v are the velocity components in x and y direction, respectively; h means the water depth; g is the acceleration of gravity; ρ is the water density; S_{xx}, S_{xy}, S_{yx} and S_{yy} are components of depth-integrated radiation stress and these variables are calculated based on the linear wave theory:

$$S_{xx}=E(n-0.5+n\cos^2\theta)\,; \tag{2a}$$

$$S_{yy}=E(n-0.5+n\sin^2\theta)\,; \tag{2b}$$

$$S_{xy}=S_{yx}=En\cos\theta\sin\theta\,. \tag{2c}$$

In Eq. (2) E means the wave energy which is calculated as:

$$E=\frac{1}{8}\rho gH^2\,, \tag{3}$$

where, H is the wave height, and the root-mean-square wave height is used for random waves following Thorton and Guza (1986). n is defined as:

$$n=0.5\left[1+\frac{2kh}{\sinh(2kh)}\right], \tag{4}$$

in which, k denotes the wave number and can be described as $k=2\pi/L$, where L means the wave length and θ is the wave direction.

In Eq. (1), R_{xx}, R_{xy}, R_{yx} and R_{yy} denote components of the roller stress; τ_{bx} and τ_{by} are bottom stresses in x and y direction, respectively; ν_{cw} means the horizontal viscosity coefficient under combined waves and currents. Calculation of these variables will be discussed in detail in the following sections.

The finite volume method is employed to discretize Eq. (1) and the modified fourth-order Runge–Kutta time-stepping scheme is applied in time integration (Chen *et al*., 2003). Detail information on numerical scheme can be referenced to Chen *et al*. (2003, 2007).

2.2 Surface Roller

The surface roller is the turbulent water volume with white foams generated in the front of wave crest after wave breaks. Svendsen (1984a, 1984b) demonstrated the concept of surface roller and introduced it in modeling wave setup and undertow. According to Svendsen (1984a), the effect of the surface roller on wave-induced nearshore circulation is indispensable because it is difficult to yield a proper description of the excess momentum flux adopting conventional wave theory in the surf zone. In momentum equations described above, contributions of the surface roller on the momentum flux are incorporated in the form of the roller stress. Following Tajima and Madsen (2006), components of the roller stress R_{xx}, R_{xy}, R_{yx}, and R_{yy} can be evaluated from the kinetic energy of surface roller E_r:

$$R_{xx} = 2E_r \cos^2\theta ; \tag{5a}$$

$$R_{xy} = R_{yx} = 2E_r \cos\theta \sin\theta ; \tag{5b}$$

$$R_{yy} = 2E_r \sin^2\theta . \tag{5c}$$

In Svendsen's (1984a) derivation, E_r is related to the area of the surface roller A_r:

$$E_r = \frac{1}{2}\frac{\rho A_r}{L}c^2 = \frac{\rho A_r}{2T}c , \tag{6}$$

in which, c means the wave celerity, and T is the wave period. It should be mentioned that the density of the surface roller equal to that of water is adopted in the derivation of Eq. (6). However, the surface roller is actually a mixture of air and water, and the density of surface roller ρ_r should be smaller than that of water. Referring to Xie (2011), ρ is substituted by ρ_r in Eq. (6) and E_r becomes

$$E_r = \frac{\rho_r A_r}{2T}c . \tag{7}$$

Earlier researches (Duncan, 1981; Okayasu *et al*., 1986) related A_r to basic wave parameters. However, the creation of the roller at the breaking point and its area increasing by absorbing part of the wave energy cannot be described properly employing this method. Based on the conservation of energy, Dally and Brown (1995) proposed a relationship among the organized wave energy, the kinetic energy of the surface roller and an energy-dissipation term:

$$\frac{\mathrm{d}\overline{F}_w}{\mathrm{d}x} + \frac{\mathrm{d}}{\mathrm{d}x}\left[\frac{1}{2}\rho_r(\beta_c c)^2\frac{A_r}{T}\right] = -\frac{\rho_r g A_r \beta_D}{T} , \tag{8}$$

where, F_w denotes the wave energy flux, and the overbar denotes time-averaging over one wave period, the second term on the left means the gradient of the kinetic energy of the surface roller, the right-hand term describes the dissipation of energy, the coefficient β_c is expected to be of order 1.0, and β_D is a dissipation coefficient related to the inclination angle of the surface roller. There are two main advantages using this energy-based formula. First, the evolution of the surface roller can be predicted in a proper way. Second, in order to evaluate E_r using Eq. (7), $(\rho_r A_r)$ can be solved as a whole in Eq. (8)

to avoid choosing a reliable value of ρ_r.

Under the assumption that energy dissipation of surface roller equals the sum of the kinetic energy of the surface roller, and the energy is transferred to roller, Tajima and Madsen (2006) further proposed a formula similar to Eq. (8).

$$\alpha\nabla\left(\frac{1}{8}\rho g H^2 c_g \boldsymbol{n}\right)+\nabla\left(\frac{\rho_r A_r}{2T}c^2\boldsymbol{n}\right)=-\frac{K_r}{h}\frac{\rho_r A_r}{2T}c^2 . \tag{9}$$

The first term on the left represents the energy transferred to the surface roller from local waves, and α is the energy transform factor which should be in the range of 0.0 to 1.0. c_g means the wave group velocity, the vector $\boldsymbol{n}=(\cos\theta,\sin\theta)$. The second term on the left is identical to that in Eq. (8). The right-side term denotes the dissipation of energy, and the empirical coefficient K_r is related to the beach slope. Goda (2006) presented that K_r can be calculated as:

$$K_r = 0.375(0.3+2.4s), \tag{10}$$

where, s is the bottom slope, and should be 0 when $s<0$.

Both Eq. (8) and Eq. (9) simulate the evolution of the surface roller in the surf zone, although the former focuses on the conservation of energy in the whole water column (including the organized wave and the surface roller), and the latter concentrates on the energy balance only in the roller itself. There are also differences in the energy dissipation term, in Eq. (8) β_D is related to the inclination angle of roller while in Eq. (9) K_r is evaluated according to the beach slope. Note that if $\alpha=1$ and $c=\sqrt{gh}$ are applied, Eq. (9) is almost identical to Eq. (8). Both of the two methods are feasible under the condition that the empirical coefficient β_D or α is well calibrated. In this study, considering that beach slope is a crucial factor in the energy dissipation of wave breaking, Eq. (9) is adopted in modeling the evolution of the surface roller. The governing equation is identical to that reported by Xie (2010, 2011), although Xie (2010) solved A_r directly in Eq. (9), leading to the problem of determining the value of ρ_r.

2.3 Horizontal Viscosity

Following Longuet-Higgins (1970), the wave-induced horizontal viscosity term can be calculated as:

$$\nu_w = Nx_0(gh)^{0.5}, \tag{11}$$

in which, N is a constant, and x_0 means the distance from the shoreline. ν_w denotes the horizontal viscosity caused by waves. Larson and Kraus (1991) proposed another empirical formula expressed as:

$$\nu_w = \lambda u_m H , \tag{12}$$

where, λ is an empirical coefficient representing the lateral mixing strength, and u_m denotes the maximum orbital velocity of waves, which can be calculated as :

$$u_m = \frac{gHT}{2L\cosh(kh)}, \tag{13}$$

Larson and Kraus (1991) reported that ν_w goes to zero in deep water, and Eq. (12) is suitable for barred beaches for the reason that ν_w is related to the wave height. In this paper Eq. (12) is employed to calculate the wave-induced horizontal viscosity coefficient.

It should be noted that the horizontal mixing is affected both by waves and currents, therefore it is considered as a combination of current-induced and wave-induced value following van Rijn (2007):

$$\nu_{cw} = \sqrt{\nu_c^2 + \nu_w^2}\ . \tag{14}$$

The current-induced horizontal viscosity is calculated based on Smagorinsky (1963) by

$$\nu_c = CA\sqrt{\left(\frac{\partial u}{\partial x}\right)^2 + \left(\frac{\partial v}{\partial y}\right)^2 + 0.5\left(\frac{\partial v}{\partial x} + \frac{\partial u}{\partial y}\right)^2}\ , \tag{15}$$

in which, C is a constant which is set as 0.25 referring to Chen *et al*. (1999), and A means the area of the computational element.

2.4 Bottom Shear Stress

In this paper, the mean bed shear stress under combined waves and currents is determined according to Soulsby (1997) which is described as:

$$\tau_m = \tau_c\left[1 + 1.2\left(\frac{\tau_w}{\tau_c + \tau_w}\right)^{3.2}\right], \tag{16}$$

where, τ_m is the mean bed shear stress during a wave cycle, and τ_c and τ_w are the bed shear stress due to current alone and to wave alone, respectively. τ_c and τ_w can be calculated by

$$\tau_c = \rho C_D \overline{U}^2; \tag{17}$$

$$\tau_w = \frac{1}{2}\rho f_w u_m^2\ , \tag{18}$$

where C_D is the drag coefficient calculated as $C_D = 0.40/[1+\ln(z_0/h)]^2$; $\overline{U}$ denotes the depth-averaged current speed; z_0 means the bed roughness length which can be calculated from the roughness height as $z_0 = k_s/30$. The wave friction factor f_w is expressed as $f_w = 1.39(A_m/z_0)^{-0.52}$ according to Soulsby (1997). A_m means the semi-orbital excursion described as $A_m = u_m T/(2\pi)$. Eq. (16) is an empirical formula which is developed based on a large data set under various wave and current conditions, and effects of the angle between waves and currents are not included in Eq. (16) considering that τ_m is the time-averaged shear stress during a wave cycle.

3. Sensitivity Analysis

In this section, effects of the roller transfer factor α in Eq. (9) and the empirical coefficient λ in Eq. (12) on wave-induced longshore current are investigated through sensitivity tests. Laboratory measurements of Experiment 4 reported by Visser (1991) are employed here as comparisons with the computed results. The experiment was carried out in a 34 m wide, 16.6 m long wave basin. The water

depth at the wave generator was 0.35 m, and the beach slope was 1/20. Regular waves were generated and the initial wave height was 0.078 m, the wave period was 1.02 s, and the initial wave direction was 15.4° respective to the cross-shore direction.

For driving the model, the measured wave heights are utilized in calculating radiation stress, so that calibration of α and λ will not be affected by any deviations of the calculated wave heights. Additionally, the Snell's law is adopted to estimate wave directions for the same reason. The measured wave height in the cross-shore direction is illustrated in Fig. 1 where x is the cross-shore coordinate originated at the shore and taken the positive offshore.

In Visser's (1991) experiment, a smooth concrete beach was constructed. Hence, in this study, a relatively small value of the roughness height k_s = 0.001 m is adopted in evaluating the bed shear stress. Actually, Goda (2006) stated that the method of evaluating the bed shear stress had a far less influence on the prediction of the longshore current compared with effects of the horizontal viscosity and the surface roller.

3.1 Effects of the Roller Transfer Factor

The value of the roller transfer factor α in Eq. (9) has been investigated by some researchers so far. Tajima and Madsen (2006) suggested that $\alpha = 0.5$, nevertheless, Goda (2006) reported that 0.5 should be the upper limit of α, and smaller value should be adopted under swell conditions. Xie (2010) reported that α should be in the range of 0.3–0.6 in simulating wave-induced currents. Different wave transformation models were employed by Tajima and Madsen (2006) and Goda (2006), which may lead to differences in α. To prevent the shortcomings of a wave model, Xie (2010) adopted measured wave heights in analyzing the effects of α, however, another tunable parameter ρ_r was introduced in his model which increased the complexity. Actually, $(\rho_r A_r)$ can be solved as a whole in Eq. (9) to avoid choosing a reliable value of ρ_r as described in Section 2.2.

In order to study the effect of α, $\lambda = 0.6$ is adopted, and α is changed from 0.0 to 0.6. Simulated results compared with Visser's (1991) measurements are illustrated in Fig. 1.

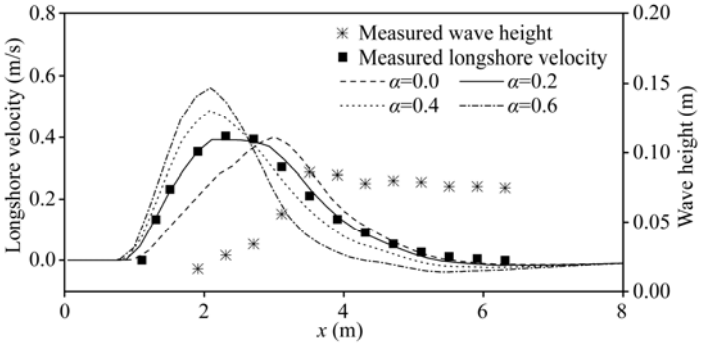

Fig. 1. Influence of α when $\lambda = 0.6$.

It is indicated that if the effects of the surface roller are ignored, that is, applying $\alpha = 0.0$ in the simulation, the profile of the longshore currents cannot suit the measured data especially in the shoreward side of the breaking point. The maximal value of the longshore velocity increases, and the

position of the peak value moves shoreward as α increases. While using $\alpha = 0.6$, simulation results are evidently inappropriate in comparison with measured data. As shown in Fig. 1, the appropriate value of α should be 0.2.

3.2 Effects of the Horizontal Mixing Coefficient

Effects of the horizontal mixing are investigated by changing λ from 0.4 to 1.0 while α is set to be 0.2. Simulated longshore currents compared with measured data are illustrated in Fig. 2. Profiles of the longshore currents are smoothed by large horizontal mixing especially on the seaward side of the breaking point. Large value of λ leads to a small peak value of the longshore velocity, although the position of the maximal value is almost immovable while changing the value of λ.

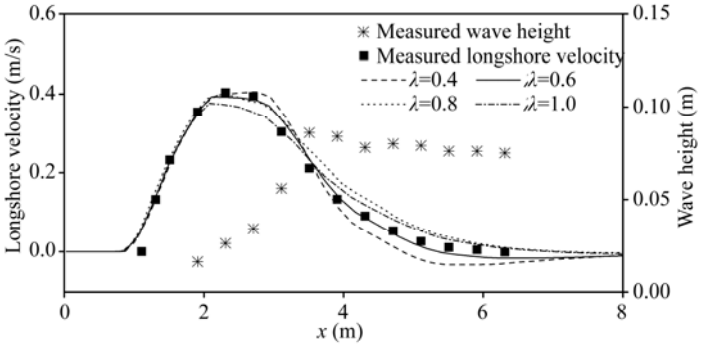

Fig. 2. Influence of λ when $\alpha = 0.2$.

Discussions on λ have been presented by a number of researchers. Range of 0.3 to 0.5 was recommended by Larson and Kraus (1991) both under laboratory conditions and in the field. Sun *et al*. (2002) applied that λ = 0.85 in their simulation. Goda (2006) suggested that λ should be in the range of 0.05 to 0.1 under laboratory conditions and 0.5 to 1.0 for field data. Zhang *et al*. (2013) employed λ = 0.5 in estimating wave-induced longshore currents. In this study, it is found that 0.6 appears to be the appropriate value of λ. Actually, different values of λ do not make remarkable differences on the profile of the longshore velocity as shown in Fig. 2.

4. Model Validation

Following the results of the sensitivity tests in the last section, empirical coefficients $\alpha = 0.2$ and $\lambda = 0.6$ are appropriate in modeling wave-induced longshore currents. Further, it is essential to examine the predictive capability of this model under various conditions by adopting these values. In this section, comparisons are made between numerical results and observations from three sets of laboratory cases and one field case. Brief conditions of these measurements are listed in Table 1, where H means the wave height at the wave generator for regular waves and the root-mean-square wave height for irregular waves, D denotes the water depth at the wave generator for the laboratory case or offshore water depth for the field case, and T is the average wave period or the peak period for regular waves or irregular waves, respectively. For the field case (Wu *et al*., 1985), the wave height and the

wave period in the deep water are presented in Table 1. Detail information will be described in the following sections.

In the following numerical simulations, the roller transfer factor α and the viscosity coefficient λ are taken as 0.2 and 0.6, respectively. For laboratory cases, the roughness height k_s = 0.001 m is used as in Section 3. For the field case, no information on sediment properties was presented by Wu *et al*. (1985), thus, k_s is specified to be a relatively large value 0.05 m approximately.

Table 1 General information of measured data

Literature	Data type	Case number	Wave type	H (m)	D (m)	T (s)	Slope
Hamilton and Ebersole (2001)	Laboratory	Test 6N	Regular	0.182	0.67	2.5	0.033
Hamilton and Ebersole (2001)	Laboratory	Test 8E	Irregular	0.159	0.67	2.5	0.033
Seabergh *et al*. (2005)	Laboratory		Regular	0.04	0.33	1.56	0.016
Wu *et al*. (1985)	Field	Feb. 4, 1980	Irregular	0.52	9.25	14.2	0.041

For driving the longshore current model, the numerical model SWAN (Booij *et al*., 1999) based on the wave action balanced equation is used to provide wave fields. It should be addressed that the wave-current interaction plays an essential role on nearshore circulations. Hence, in this study coupling between the wave model and the flow model is employed as the following steps: (1) wave fields are computed by SWAN; (2) then the output from SWAN such as wave heights wave directionsand wave length are employed to calculate the radiation stresses and further wave-induced hydrodynamics in the flow model; (3) after that, currents and the water level simulated by the flow model are transmitted to SWAN; (4) the former two steps are repeated again, and the final current fields are obtained.

4.1 Laboratory Measurements Presented by Hamilton and Ebersole (2001)

Several series of laboratory experiments on wave-induced longshore currents were carried out by Hamilton and Ebersole (2001) at the U.S. Army Engineer Research and Development Center. The wave basin was 30 m wide and 50 m long, and the water depth was 0.667 m at the wave generator. Regular and irregular waves were generated in Test 6N and Test 8E, respectively. Incident wave conditions are summarized in Table 1. External circulation system was constructed, and high degree of longshore uniformity was obtained in their observations. Wave heights and the longshore velocity were measured along the cross-shore direction.

Fig. 3 illustrates simulated wave heights and longshore currents along with the measured data of Test 6N. x is the cross-shore coordinate originated at the shore and taken the positive offshore. As shown in Fig. 3a, the predicted wave height at the breaking point is slightly underestimated by the wave model SWAN, however, the position where wave breaks is well captured. In Fig. 3b, calculations of longshore currents agree well with the measurements by applying recommended empirical coefficients described above.

Computed wave heights and longshore currents in comparison with measured data of Test 8E are presented in Fig. 4. Results of SWAN agree fairly well with the measured wave heights in Fig. 4a where the root-mean-sqare wave heights are presented. However, underestimation of the longshore velocity can be detected at the position where the measured longshore velocity reaches its maximum.

The simulated profile of the longshore current is supposed to be smoother than the measurements of Test 8E. It can be interpreted that effects of the horizontal mixing is somehow larger in our simulation for the irregular waves. Thornton and Guza (1986) pointed out that effects of the horizontal mixing could be neglected in numerical models for random waves. Additionally, the radiation stress is calculated by the root-mean-square wave for the random wave case which may be one of the main reasons for the differences between numerical results and the measurements. By comparing the profile of the measured wave height between Fig. 3a and Fig. 4a, the gradient of the wave height in Fig. 3a near the breaking point is significant. In contrast, the breaking point is inconspicuous as shown in Fig. 4a, indicating a small gradient of the radiation stress which may lead to a much smoother profile of the longshore velocity.

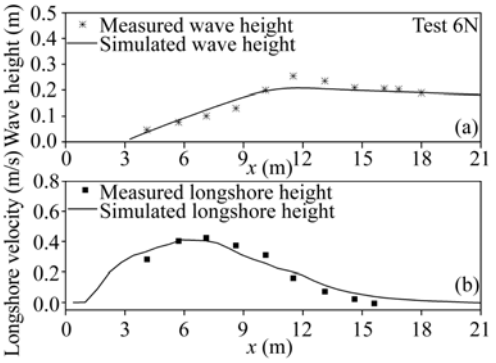

Fig. 3. Numerical results in comparison with measured data of Test 6N: (a) wave height; (b) longshore velocity.

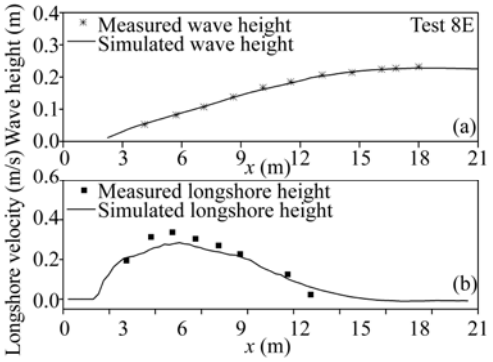

Fig. 4. Numerical results in comparison with measured data of Test 8E: (a) wave height, (b) longshore velocity.

4.2 Laboratory Observations on An Ideal Inlet Presented by Seabergh *et al*. (2005)

Coastal inlets on sandy coasts are often controlled by jetties for maintaining navigation. Longshore current interrupted by jetties lead to complex circulation pattern in the vicinity of the inlet which is the major driving force of the sediment transport and further erosion or accumulation of shoreline. In this section, the performance of our wave-induced current model on an ideal inlet will be examined. Additionally, one of the major objectives of this paper is to develop a numerical model with unstructured grids which makes the model more effective and convenient to handle irregular coastal geometry. In this simulation, computational grids will be refined around the inlet channel.

Laboratory experiments on the hydrodynamics in the vicinity of the inlet channel were carried out by Seabergh *et al*. (2005). The sketch of the bathymetry is illustrated in Fig. 5. Detail measurements on waves and currents were made, and these valuable data will be employed to test the reliability of our model.

During the experiment, regular waves were generated on the west boundary with an incident angle of 20° relative to the cross-shore direction. Incident wave conditions are presented in Table 1. Both reflecting and absorbing jetties were adopted in the experiment, while in the numerical model the jetty was treated as an absorbing structure. Hence, numerical results will be compared with the measurements for the case with absorbing jetties. Computational grids in the vicinity of jetties are shown in Fig. 6.

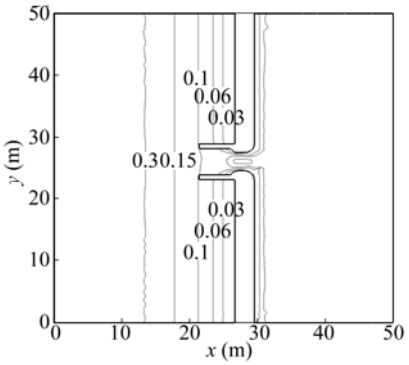

Fig. 5. Sketch of the bathymetry presented by Seabergh *et al*. (2005).

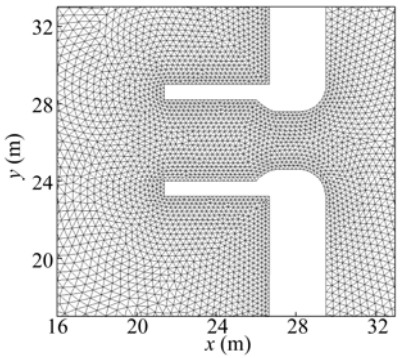

Fig. 6. Computational grids in the vicinity of jetties.

Locations of a part of wave gauges are presented in Fig. 7. For further details on the experiment, see Seabergh *et al*. (2005) and Zheng *et al*. (2011). Simulated wave heights along transect T1–T4 in comparison with the measured data are illustrated in Fig. 8. Numerical results of SWAN agree acceptable well with the observations.

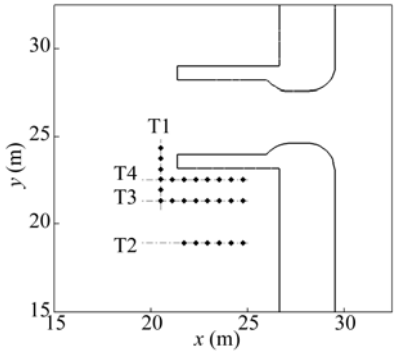

Fig. 7. Locations of wave gauges transect lines T1–T4.

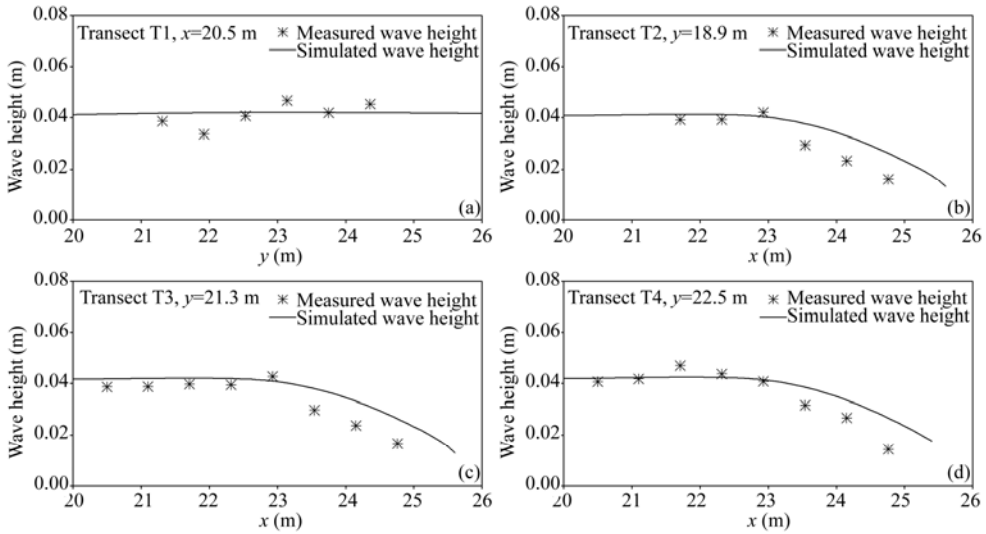

Fig. 8. Computed and measured wave heights along (a) Transect T1, (b) Transect T2, (c) Transect T3, and (d) Transect T4.

Simulated wave-induced circulations near the jetties are shown in Fig. 9. Longshore currents from south to north are interrupted by jetties, and clockwise vortex appears in the sheltered region of the northern jetty. A comparison between computed results and the measured velocity is shown in Fig. 10. Numerical results compare reasonably well with the measurements, although some deviations still can be detected. Simulated circulation pattern is supposed to be reasonable by utilizing the computational coefficients presented above.

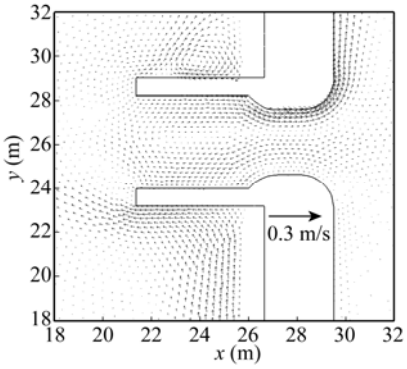

Fig. 9. Numerical circulation pattern in the vicinity of jetties.

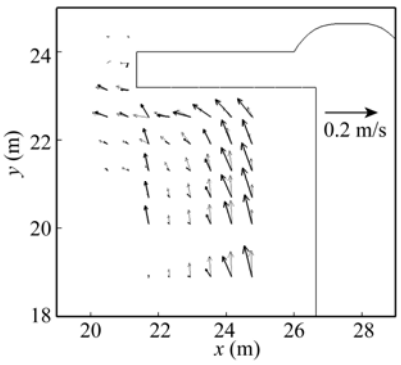

Fig. 10. Simulated velocity (thin dash arrows) compared with the measured data (coarse solid arrows).

4.3 Field Measurements Presented by Wu *et al.* (1985)

Field measurements on longshore currents were carried out by Wu *et al*. (1985) at Leadbetter Beach, California. Cross-shore distributed wave conditions and longshore velocity were measured during February 2–6, 1980. In this study, measurements on Feb. 4 were used for validation of the model, and monochromatic and unidirectional waves were obtained in this case. The sketch of bathymetry is shown in Fig. 11, and the bottom contours are almost parallel to the shoreline. Offshore wave conditions are listed in Table 1. The incident wave angle is 19.1° relative to the cross-shore direction.

Comparisons between simulated results and the measured data are presented in Fig. 12 in which y is the cross-shore coordinate originated at the shore and taken the positive offshore.

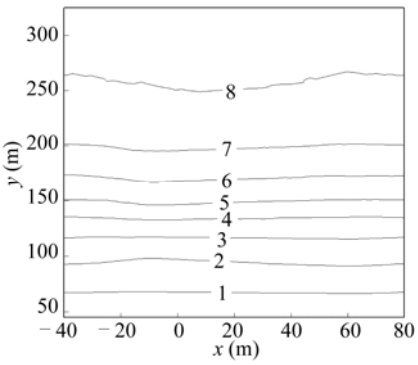

Fig. 11. Contours at the Leadbetter Beach.

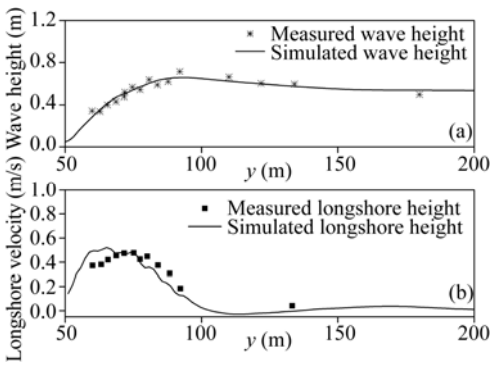

Fig. 12. Numerical results in comparison of measured data: (a) wave height; (b) longshore velocity.

As shown in Fig. 12a, computed wave heights agree reasonably well with the measurements. In

Fig. 12b, the shape of the cross-shore distribution of the longshore current is more or less in accordance with the measured data, although overestimations can be detected at the most shoreward gauges. Small differences between computed wave heights and the measured data at the most shoreward wave gauges are responsible for the overestimation of the longshore velocity. The wave model fails to simulate the regeneration of the wave height at the two most shoreward gauges which results in a larger gradient of the radiation stresses in the numerical model and further an overestimation of longshore velocity. With the complex condition in the field, numerical results of the longshore velocity are still supposed to be acceptable.

5. Conclusions

A depth-integrated numerical model for simulating wave-induced longshore currents has been developed with unstructured grids. Effects of the horizontal mixing under waves and currents have been included. A modified equation based on Tajima and Madsen (2006) has also been introduced to describe the transformation of the surface roller.

Sensitivity tests have been made in order to study effects of the surface roller and the horizontal mixing. According to the results of numerical experiments, the horizontal mixing plays an important role in smoothing the profile of longshore currents while the surface roller can significantly shift longshore currents shoreward, and enhance the peak value of the longshore velocity. Empirical coefficients $\alpha = 0.2$ in Eq. (9) and $\lambda = 0.6$ in Eq. (12) are recommended in the simulation of wave-induced longshore currents.

In order to examine the performance of this model, three sets of laboratory measurements and one set of field observation data have been employed as comparisons while applying recommended value of computational coefficients. Simulated results show generally good agreements with measured data, although small differences do exist. The presented model will be utilized to calculate the longshore sediment transport and shoreline evolution in the future.

References

Artagan, S. S., 2006. *A one-Line Numerical Model for Shoreline Evolution Under the Interaction of Wind Waves and Offshore Breakwaters*, Ph.D. Thesis, Middle East Technical University.

Baykal, C., Ergin, A. and Güler, I., 2014. Two-dimensional depth-averaged beach evolution modeling: Case study of the Kızılırmak River mouth, Turkey, *J. Waterw. Port Coast. Ocean Eng.*, ASCE, **140**(3): 05014001-1–05014001-15.

Booij, N., Ris, R. C. and Holthuijsen, L. H., 1999. A third-generation wave model for coastal regions: 1. Model description and validation, *J. Geophys. Res.*, **104**(C4): 7649–7666.

Chen, C., Huang, H., Beardsley, R. C., Liu, H., Xu, Q. and Cowles, G., 2007. A finite volume numerical approach for coastal ocean studies: Comparison with finite difference models, *J. Geophys. Res.*, **112**(C3): C3018.

Chen, C., Liu, H. and Beardsley, R. C., 2003. An unstructured grid, finite-volume, three-dimensional, primitive equations ocean model: Application to coastal ocean and estuaries, *J. Atmos. Oceanic Technol.*, **20**(1): 159–186.

Chen, Q., Dalrymple, R. A., Kirby, J. T., Kennedy, A. B. and Haller M. C., 1999. Boussinesq modeling of a rip

current system, *J. Geophys. Res.*, **104**(C9): 20617–20637.

Cui, L., Tang, J. and Sheng, Y. M., 2008. Numerical simulation of wave field and coastwise current in alongshore zone, *Chinese Journal of Hydraulic Engineering*, **39**(12): 1340–1345. (in Chinese)

Cui, L., Tong, F. F. and Shi, F., 2011. Numerical simulation of wave-induced currents combined with parabolic mild-slope equation in curvilinear coordinates, *China Ocean Eng.*, **25**(3): 457–468.

Dabees, M. and Kamphuis, J. W., 1998. ONELINE, a numerical model for shoreline change, *Proceedings of the 26th International Conference on Coastal Engineering*, Copenhagen, Denmark, 2668–2681.

Dally, W. R. and Brown, C. A., 1995. A modeling investigation of the breaking wave roller with application to cross-shore currents, *J. Geophys. Res.*, **100**(C12): 24873–24883.

Ding, Y., Wang, S. S. Y. and Jia, Y., 2006. Development and validation of a quasi-three-dimensional coastal area morphological model, *J. Waterw. Port Coast. Ocean Eng.*, ASCE, **132**(6): 462–476.

Duncan, J. H., 1981. An experimental investigation of breaking waves produced by a towed hydrofoil, *Proceedings of the Royal Society of London A: Mathematical and Physical Sciences*, **377**(1770): 331–348.

Goda, Y., 2006. Examination of the influence of several factors on longshore current computation with random waves, *Coast. Eng.*, **53**(2-3): 157–170.

Hamilton, D. G. and Ebersole, B. A., 2001. Establishing uniform longshore currents in a large-scale sediment transport facility, *Coast. Eng.*, **42**(3): 199–218.

Kuriyama, Y., and Ozaki, Y., 1993. Longshore current distribution on a bar trough beach – Field measurements at HORF and numerical model, *Rep. Port Harb. Res. Inst.*, **32**(3): 3–37.

Larson, M. and Kraus, N. C., 1991. Numerical model of longshore current for bar and trough beaches, *J. Waterw. Port Coast. Ocean Eng.*, ASCE, **117**(4): 326–347.

Longuet-Higgins, M. S. and Stewart, R. W., 1962. Radiation stress and mass transport in gravity waves, with application to "surf beats", *J. Fluid Mech.*, **13**(04): 481–504.

Longuet-Higgins, M. S., 1970. Longshore currents generated by obliquely incident sea waves: 1, *J. Geophys. Res.*, **75**(33): 6778–6789.

Murray, A. B. and Ashton, A., 2004. Extending a 1-line modeling approach to explore emergent coastline behavior, *Proceedings of the 29th International Conference on Coastal Engineering*, Lisbon, Portugal, 2035–2047.

Nam, P. T., Larson, M. and Hanson, H., 2009. A numerical model of nearshore waves, currents, and sediment transport, *Coast. Eng.*, **56**(11): 1084–1096.

Okayasu, A., Shibayama, T. and Mimura, N., 1986. Velocity field under plunging waves, *Proceedings of the 20th International Conference on Coastal Engineering*, Taipei, 660–674.

Reniers, A. J. H. M. and Battjes, J. A., 1997. A laboratory study of longshore currents over barred and non-barred beaches, *Coast. Eng.*, **30**(1-2): 1–22.

Seabergh, W. C., Lin, L. and Demirbilek, Z., 2005. *Laboratory Study of Hydrodynamics Near Absorbing and Fully Reflecting Jetties*, Coastal and Hydraulics Laboratory Technical Report ERDC/CHL-TR-05-8, U.S. Army Engineer Research and Development Center, Vicksburg, MS.

Smagorinsky, J., 1963. General circulation experiments with the primitive equations, I. the basic experiment, *Mon. Weather Rev.*, **91**(3): 99–164.

Smith, J. M., Larson, M. and Kraus, N. C., 1993. Longshore current on a barred beach: Field measurement and calculation, *J. Geophys. Res.*, **98**(C12): 22717–22731.

Soulsby, R., 1997. *Dynamics of Marine Sands*, London, Thomas Telford.

Sun, T., Han, G. and Tao, J. H., 2002. Numerical simulation of wave-induced long-shore currents and experimental verification, *Chinese Journal of Hydraulic Engineering*, **11**, 1–7. (in Chinese)

Svendsen, I. A., 1984a. Wave heights and set-up in a surf zone, *Coast. Eng*., **8**(4): 303–329.

Svendsen, I. A., 1984b. Mass flux and undertow in a surf zone, *Coast. Eng*., **8**(4): 347–365.

Tajima, Y. and Madsen, O. S., 2006. Modeling near-shore waves, surface rollers, and undertow velocity profiles, *J. Waterw*. *Port Coast. Ocean Eng.*, ASCE, **132**(6): 429–438.

Thornton, E. B. and Guza, R. T., 1986. Surf zone longshore currents and random waves: Field data and models, *J. Phys. Oceanogr.*, **16**(7): 1165–1178.

Treffers, R., 2008. *Wave-Driven Longshore Currents in the Surf Zone*, MSc. Thesis, Delft University of Technology.

van Rijn, L. C., 2007. Unified view of sediment transport by currents and waves. II: Suspended Transport, *J. Hydraul. Eng.*, **133**(6): 668–689.

Visser, P. J., 1991. Laboratory measurements of uniform longshore currents, *Coast. Eng*., **15**(5-6): 563–593.

Wu, C. S., Thornton, E. B. and Guza, R. T., 1985. Waves and longshore currents: comparison of a numerical model with field data, *J. Geophys. Res*., **90**(C3): 4951–4958.

Xie, M., 2010. *Three Dimensional Modeling of Current and Sediment Transport for Muddy Coasts Coupling with Waves and Tidal Flow*, Ph.D. Thesis, Hohai University. (in Chinese)

Xie, M., 2011. Establishment, validation and discussions of a three dimensional wave-induced current model, *Ocean Model*., **38**(3-4): 230–243.

Zhang, C., Wang, Y. G. and Zheng, J. H., 2009. Numerical study on vertical structures of undertow inside and outside the surf zone, *Acta Oceanol. Sin*., **28**(5): 103–111.

Zhang, M. L., Wu, W. M., Lin, L. H. and Yu, J. N., 2012. Coupling of wave and current numerical model with unstructured quadtree grid for nearshore coastal waters, *Sci. China Tech. Sci*., **55**(2): 568–580.

Zhang, W., Deng, J., Harff, J, Schneider, R. and Dudzinska-Nowak, J., 2013. A coupled modeling scheme for longshore sediment transport of wave-dominated coasts – A case study from the southern Baltic Sea, *Coast. Eng.*, **72**, 39–55.

Zheng, J. H., Nguyen, V. T. and Zhang, C., 2011. Spectral wave transformation model for simulating refraction-diffraction with strongly reflecting coastal structures, *Acta Oceanol. Sin*., **30**(2): 25–32.

Zheng, J. H. and Tang, Y., 2009. Numerical simulation of spatial lag between wave breaking point and location of maximum wave-induced current, *China Ocean Eng*., **23**(1): 59–71.

Zheng, J. H., Wang, T. W., Wang, G., Zhang, C. M. and Zhang, C., 2012. Iteration coupling simulation of random waves and wave-induced currents, *J. Applied Mathematics*, 2012, Article ID 205376.

Zheng, J. H., Zhang, C., Demirbilek, Z. and Lin, L., 2014. Numerical study of sandbar migration under wave-undertow interaction, *J. Waterw*. *Port Coast*. *Ocean Eng*., ASCE, **140**(2): 146–159.